General Disclaimer

One or more of the Following Statements may affect this Document

- This document has been reproduced from the best copy furnished by the organizational source. It is being released in the interest of making available as much information as possible.

- This document may contain data, which exceeds the sheet parameters. It was furnished in this condition by the organizational source and is the best copy available.

- This document may contain tone-on-tone or color graphs, charts and/or pictures, which have been reproduced in black and white.

- This document is paginated as submitted by the original source.

- Portions of this document are not fully legible due to the historical nature of some of the material. However, it is the best reproduction available from the original submission.

NASA TM X- 71051

RADIATIVE TRANSFER IN A PLANE STPATIFIED DIELECTRIC

THOMAS T. WILHEIT, Jr.

MARCH 1975

RADIATIVE TRANSFER IN A
PLANE STRATIFIED DIELECTRIC

Thomas T. Wilheit, Jr.

March 1975

GODDARD SPACE FLIGHT CENTER
GREENBELT, MARYLAND

CONTENTS

ILLUSTRATIONS

TABLES

RADIATIVE TRANSFER IN A
PLANE STRATIFIED DIELECTRIC

Thomas T. Wilheit, Jr.

ABSTRACT

A model is developed for calculating radiative transfer in a stratified dielectric. This model is used to show that the reflectivity of a stratified dielectric is primarily determined by gradients in the real part of the refractive index over distances on the order of 1/10 wavelength in the medium. The effective temperature of the medium is determined by the thermodynamic temperature profile over distances of the order δ_T where

$$\int_0^{\delta_T} \text{Im}(n) \, dx = \lambda / 4\pi$$

RADIATIVE TRANSFER IN A
PLANE STRATIFIED DIELECTRIC

Thomas T. Wilheit, Jr.

There is a burgeoning interest in microwave remote sensing of the Earth's surface. The dominant theme of both active (Radar) and passive (Radiometer) systems is a variability of the dielectric properties of the surface as a function of a number of parameters of interest. It is straightforward to calculate the reflectivity and microwave radiance of an interface between two homogenous dielectrics using the Fresnel relations (Panofsky and Phillips, 1962). However, quantitative understanding of many measurements requires consideration of a more sophisticated model than a simple planar, isothermal dielectric interface. It is the purpose of this document to develop a framework for consideration of dielectric and thermal variations in one dimension. To this end, we will develop a theory of radiative transfer in a planar layered medium and demonstrate that this layered theory is useful for consideration of continuously varying dielectrics.

In the first section, we solve the field equations for a multiple layered dielectric to provide a framework for the second section wherein we solve the radiative transfer problem. In the third section, we calculate the thermal radiation from each layer and thus solve the radiative transfer problem. In the last section, we apply this theory to certain specific cases.

Electric Fields within a Layered Medium

Consider a series of N dielectric layers, each with a complex index of refraction n_j and a thickness δ_j. The first and last layers are semi-infinite. Electromagnetic waves can propagate in each layer with the form $\vec{E} = \vec{E}_{oj} e^{i\vec{k}_j \cdot \vec{r}}$ where $\vec{k}_j$ is the propagation vector with magnitude $2\pi n_j / \lambda$, τ is the free space wavelength, j specifies the layer, and $\vec{r}$ is a general position vector. $\vec{E}_{oj}$ is an arbitrary electric vector with complex coefficients subject only to the constraint that $\vec{k}_j \cdot \vec{E}_{oj} = 0$. We will choose the coordinate system such that the interfaces are normal to the x direction. In order to satisfy any (non-trivial) boundary conditions at the interfaces, we must impose Snell's law on the k vectors;

$$\vec{k} \times \hat{x} = constant$$

where $\hat{x}$ is a unit vector in the x direction. We can then further specify that $k_y \equiv 0$ with no loss of generality. We may now consider the x dependence only in the wave and include the y and z dependence implicity in the E_0 value.

The + and - signs correspond to waves propagating in the positive and negative x directions, respectively. The value of θ_i the angle between the direction of propagation and the x direction, is related among all the layers by the Snell's law constraint, $n_j \sin \theta_j =$ constant. θ_j is, in general, a complex number. We may now establish a pair of propagator functions:

$$P^{\pm}(x) = e^{\pm(2\pi i/\lambda)\int_{x_1}^{x} n(x') \cos(\theta(x'))dx'}$$

where x_1 is the coordinate of the interface between the first and second layers.

The electric fields within the j the layer propagating in either direction can be expressed in terms of the propagator function as this function satisfies the necessary wave equation at all points.

Defining the x origin to be at the interface of the first and second layers leads to a simple form for $p_j^{\pm}$, the propagator at the interface between the j and $j+1^{\text{th}}$ layers.

$$p_j^{\pm} = e^{\pm(2\pi i/\lambda) n_j \delta_j \cos \theta_j} p_{j-1}^{\pm}$$

$$p_1^{\pm} = 1$$

The electric fields at each interface may then be expressed in terms of this propagator and are shown schematically in Figure 1. It is these fields to which the appropriate boundary conditions must be applied in order to determine the electric fields.

Any incident electric wave may be resolved into two polarizations; we will solve for two mutually orthogonal linear polarizations from which any arbitrary polarization may be synthesized by linear superposition. Horizontal polarization is defined as having the electric vector in the plane of the interfaces, whereas the vertically polarized wave has its electric field vector in the plane determined by the propagations vector and the normal to the interfaces. This definition breaks down at normal incidence but, by symmetry, the physical distinction between the two polarization breaks down as well, and the two solutions converge in the limit $\theta \to 0$. The boundary conditions to be applied are that the tangential components

of both the electric and magnetic fields be constant across the boundary. The magnetic field is related to the electric through Maxwell's equation giving:

$$\vec{H} = \vec{k} \times \vec{E}/\omega\mu$$

where ω is the angular frequency of the wave and μ the magnetic permitivity which we will assume to be the same on both sides of the boundary. Thus we have:

$$\hat{X} \times (p_j^+ \vec{E}_j^+ + p_j^- \vec{E}_j^-) = \hat{X} \times (p_j^+ \vec{E}_{j+1}^+ + p_j^- \vec{E}_{j+1}^-)$$

and

$$\hat{X} \times (p_j^+ \vec{k}_j^+ \times \vec{E}_j^+ + p_j^- \vec{k}_j^- \times \vec{E}_j^-) = \hat{X} \times (p_j^+ \vec{k}_j^+ \times \vec{E}_{j+1}^+ + p_j^- \vec{k}_{j+1}^- \times \vec{E}_{j+1}^-)$$

Using Snell's law and conventional vector analysis, these may be reduced for horizontal polarization to:

$$p_j^+ E_j^+ + p_j^- E_j^- = p_j^+ E_{j+1}^+ + p_j^- E_{j+1}^-$$

and

$$n_j \cos \theta_j (p_j^+ E_j^+ - p_j^- E_j^-) = n_{j+1} \cos \theta_{j+1} (p_j^+ E_{j+1}^+ - p_j^- E_{j+1}^-)$$

and in the vertical case to:

$$\cos \theta_j (p_j^+ E_j^+ - p_j^- E_j^-) = \cos \theta_{j+1} (p_j^+ E_{j+1}^+ + p_j^- E_{j+1}^-)$$

and

$$n_j (p_j^+ E_j^+ - p_j^- E_j^-) = n_{j+1} (p_j^+ E_{j+1}^+ - p_j^- E_{j+1}^-)$$

A result of our definition of the propagation function is that

$$p_j^+ = (p_j^-)^{-1}$$

permitting these to be further simplified

$$(p_j^+)^2 \, E_j^+ + E_j^- = (p_j^+)^2 \, E_{j+1}^+ + E_{j+1}^-$$

and

$$n_j \cos \theta_j [(p_j^+)^2 \, E_j^+ - E_j^-] = n_{j+1} \cos \theta_{j+1} [(p_j^+)^2 \, E_{j+1}^+ - E_{j-1}^-]$$

for the horizontal polarization and

$$\cos \theta_j [(p_j^+)^2 \, E_j^+ + E_j^-) = \cos \theta_{j+1} [(p_j^+)^2 \, E_{j+1}^+ + E_{j+1}^-]$$

3

and

$$n_j [(p_j^+)^2 E_j^+ - E_j^-] = n_j [(p_j^+)^2 E_{j+1}^+ - E_{j+1}^-]$$

for the vertical polarization.

For the N layers, we have N-1 interfaces with two boundary conditions so that we have a total of 2N-2 equations to solve for the 2N electric fields. We may also specify the incident radiation in the positive direction on the first interface and in the negative direction on the last interface, giving the two remaining conditions needed to determine a solution for the electric fields. Here we will specify a field of unit amplitude for the input in the positive direction and that no wave is propagating in the negative direction in the last layer. The first condition is arbitrary, but since the equations are linear, the solution may be scaled to whatever field is desired. The second condition requires either that there are no further reflection possibilities beyond the last layer considered, or that the intervening layers are sufficiently opaque that whatever field may exist is of no consequence.

We may solve this system of equations by arbitrarily specifying E_N^+ and setting $E_N^- = 0$, and then solving for E_{N-1}^+ and E_{N-1}^- using the boundary conditions for the last interface and continuing through each of the interfaces in turn. Since the resulting solution for E_1^+ is, in general, not unity and thus does not satisfy the initial condition, we must exploit the linearity of the equations and appropriately scale all the E's.

This will enable us to solve for the net reflectively of a stratified dielectric. This is sufficient in the case dealing with a strong electric field so that the thermal radiation field may be ignored. Also up to this point, nothing new has been derived. This, apart from notation, is just the result obtained in chapter II Wait (1970). However, this notation is more convenient for the radiative transfer calculations which follow.

Radiative Transfer

Consider a black body at a thermodynamic temperature t_0 in the first layer (assumed to have n = 1 + 0 i) radiating isotropically at a rate given by Boltzman's law (Kraus 1966):

$$B = \frac{2h\nu^2}{c^2} \left\{ \frac{1}{e^{h\nu/kt_0} - 1} \right\}$$

4

where B is the power per unit time per unit cross-sectional area of radiator per unit bandwidth per unit solid angle, h is Planck's constant, c the speed of light, ν the frequency, and k Boltzman's constant. For frequencies less than about 120 GHz and terrestrial temperatures ($t_0 \gtrsim 190°K$), it is accurate to better than 0.1°K to reduce this to the Rayleigh-Jeans approximation; $B = 2\nu^2 k t_0 / c^2$ so that the intensity of radiation is linearly related to the thermodynamic temperature of the radiator and may be characterized by an equivalent blackbody temperature, or brightness temperature; $T_B = BC^2/2\nu^2 k$.

Each layer absorbs a fraction k_j of this radiation, where j is the index specifying the layer. If each of these layers is also at a temperature t_0, each must also radiate as much energy to the blackbody as it absorbs from the blackbody since they are in equilibrium. Since the directional and polarization properties of the black body may be varied arbitrarily, this must hold true along any propagation path and for any polarization. Since the actual radiation from any layer except the first is independent of the presence of a blackbody in the first layer, and since the amount of radiation from any layer is independent of the temperature of any other layer, except in so far as the temperature affects the dielectric properties, then the radiation propagating in a given direction, θ, is given by

$$T_B^P(\theta) = \sum_{i=2}^{N} f_i^P(\theta) \, t_i + R^P(\theta)$$

where $f_i^P(\theta)$ is the fraction of radiation incident on the first interface at an angle θ, with polarization P, which would be absorbed by the jth layer, t_j is the thermodynamic temperature of the layer, $R^P(\theta)$ is the reflectivity for the radiation $T_{B_{inc}}^P(\theta)$ incident at an angle, θ, on the first interface. Since by conservation of energy

$$\sum_{i=2}^{M} f_i^P \theta + R^P(\theta) = 1$$

this reduces in the isothermal case to

$$T_B^P(\theta) = R^P(\theta) \, T_{B_{inc}}^P(\theta) + (1 - R^P(\theta)) \, t_0$$

The crux, then, of determining the brightness temperature which would be observed from a stratified dielectric is in calculating the $\{f_j\}$. Clearly, the value of f_j for given layer j is $(\mathcal{E}_{j-1} - \mathcal{E}_j)/\mathcal{E}_1$ where $\mathcal{E}_{j-1}$ is the net electromagnetic energy flux entering the jth layer at the j-1'st interface and $\mathcal{E}_j$ is the same for the j + 1'st layer at the j'th interface for an electromagnetic energy flux $\mathcal{E}_1$ incident on the first interface.

The electromagnetic energy flow through a plane is given by the Poynting vector $\vec{S}$ which is defined as; $\vec{S} = R_e(\vec{E} \times \vec{H}^*)$; where R_e denotes the real part of the vector product of the complex electric and magnetic fields and the asterisk (*) denotes complex conjugation. Since $\vec{H} = \vec{k} \times \vec{E}/\omega\mu$,

$$S = R_e \left\{ \frac{\vec{E} \times (\vec{k}^* \times \vec{E}^*)}{\omega\mu} \right\}$$

using this relationship, it may be shown that

$$\lambda\omega\mu\mathcal{E}_j/2\pi = R_e(n_j \cos\theta_j) \, |E_j^+ p_j|^2$$

$$+ R_e(n_j \cos\theta_j) \, |E_j/p_j|^2$$

$$+ 2 \, \text{Im}(n_j \cos\theta_j) \, \text{Im}(E_j^+ (E_j^-)^2 \, p_j/p_j^*)$$

and that

$$\lambda\omega\mu\mathcal{E}_{j-1}/2\pi = R_e(n_j \cos\theta_j) \, (E_j^+ p_{j-1})^2$$

$$+ R_e(n_j \cos\theta_j) \, |E_j^-/p_{j-1}|^2 + 2 \, \text{Im}(n_j \cos\theta_j) \, \text{Im}(E_j^+ (E_j)^* \, p_{j-1}/p_{j-1}^*)$$

and since we defined the incoming field to have unit amplitude,

$$\mathcal{E}_1 = \frac{2\pi \cos\theta_0}{\lambda\omega\mu}$$

so that

$$S_j = \frac{1}{\cos\theta_1} \left[R_e(n_j \cos\theta_j) \, |E_j^+|^2 \, (|p_{j-1}|^2 - |p_j|^2) \right.$$

$$+ R_e(n_j \cos\theta_j) \, |E_j^-|^2 \left(\left|\frac{1}{p_j}\right|^2 - \left|\frac{1}{p_{j-1}}\right|^2 \right)$$

$$\left. + 2 \, \text{Im}(n_j \cos\theta_j) \, \text{Im}\left(E_j^+ (E_j^-)^* \left(\frac{p_{j-1}}{p_{j-1}^*} - \frac{p_j}{p_j^*} \right) \right) \right]$$

6

The two terms containing $R_e(n_j \cos\theta_j)$ represent the attenuation of the forward and backward waves, respectively, and the term in $Im(n_j \cos\theta_j)$ represents the interference between the two waves.

In the appendix, listings of two FORTRAN IV subroutine, HPLD and VPLD, are presented. These subroutines solve the field equations and calculate the thermal weighting functions for the horizontal and vertical polarizations, respectively.

Sample Calculations

As an application of this theory, consider the situation shown schematically in Figure 2. This represents an abrupt change in the refractive index from n_1 to n_2, then a continuous linear change from n_i to n_2 over a distance δ and a constant index beyond that.

This is a common situation for the air/soil interface where n_0 is the refractive index of air and n_2 is the refractive index in the deeper, homogenous part of the soil; n_1 corresponds to the surface of the soil which has been dried by evaporation or moistened by condensation. In Table I, the values for n_1 and n_2 and corresponding moisture values for four different cases are given. These indices of refraction are typical of a clay loam soil at a wavelength of 19.35 GHz and were, along with the choice of moisture values, extracted from Schmugge et al (1974).

It is obvious that if δ is long enough ($\delta \gg \lambda$),the surface reflectivity would be just that produced by the $n_0 - n_1$ interface and if $\delta \ll \lambda$, the reflectivity is just the $n_0 - n_2$ reflectivity. The question remains of how the reflectivity behaves when $\delta \approx \lambda$ and from what depth the thermal emission comes.

For each of the three sets of indices, this arrangement was approximated by a number of layers (10, 20, 40, 80, and 160), the reflectivities and temperature weighting functions were calculated for normal incidence and for both horizontal and vertical polarization at 45° incidence, and δ was varied from $\lambda/100$ to 10λ. In each case, the result for 160 layers was compared with each result for fewer layers. The results are shown in Table 2 for the maximum difference observed for any δ for each of the models. The reflectivity error between the result for 80 and for 160 layers was, in no case, greater than .0017, which corresponds to a brightness temperature error of only about 0.5°K, or in the case of a radar measurement, an error of less than 0.05 dB. The 0.5°K value is about the accuracy achievable in current state-of-the-art radiometric measurements, and the 0.05 dB value is about an order of magnitude better than the state-of-the-art in radar measurements. Thus the convergence of this stepwise approximation to accuracies relevant to interpretation of experiments is quite rapid.

In Figure 3, the reflectivity results for viewing perpendicularly to the interface in all four cases are plotted. In each case, for $\delta \gtrsim 3$, the reflectivity is essentially that of the $n_0 - n_1$ interface only and for $\delta/\lambda \lesssim 1/30$, the reflectivity approaches that of the subsurface layer assymptotically. There is a rather abrupt transition region between these values of δ/λ. On the large δ side of this transition, small local maxima and minima in reflectivity are observed. These correspond to electrical lengths for the transition region, $R_e (n_1 + m_2)\delta/2$, of $1/2$ and $1/4$ wavelength, respectively, for the first three cases. The positions of the minimum and the maximum are reversed for the fourth case. Between this quarter wave resonance and $\delta \approx \lambda/30$, the reflectivity changes rapidly from a value characteristic of n_1 to a value characteristic of n_2. We can define a reflectivity sampling depth δ_r for this profile, as the value of δ at which the reflectivity is that which would result from an abrupt change in the index of refraction from 1 to $(n_1 + n_2)/2$. The values of δ_r are given in Table 3 for each of the four models for perpendicular viewing and for viewing at $45°$ incidence angle for both horizontal and vertical polarizations. The sampling depths range from $.073\lambda$ to $.032\lambda$. The shorter sampling depths correspond roughly to the larger indices of refraction. The sampling depths were multiplied by the average real part of the refractive index $\langle n_r \rangle$ through the transition region; these results are also given in Table 2. These values show little variation from a minimum of 0.132 to a maximum of 0.162 for the first three cases. They are somewhat smaller for the wet surface case.

It is of particular interest to note the lack of significant angular dependence. This occurs because the direction of propagation through the medium remains nearly normal to the interface even for oblique incidence as a result of Snell's law. The decrease of the angular effect with increasing dielectric constant is consistent with this interpretation.

It is also possible to calculate the average depth at which the thermal radiation upwelling from the soil originates. We will call this the thermal sampling depth, δ_T, and it is given by

$$\delta_T = \frac{\sum x_i f_i}{\sum f_i}$$

where x_i is the depth of the ith layer and f_i is the weighting function for that layer as previously defined. It is readily shown for a uniform dielectric $(n_1 = n_2)$ that

$$\delta_T = \frac{\lambda}{4\pi \, Im(n)}$$

This may be generalized as an approximation to δ_T to aid in understanding the physics of the problem. We define δ_T' such that

$$4\pi \int_0^{\delta_T'} \text{Im}(n)\, dx = \lambda$$

In Figure 4, the values of δ_T (solid line) and δ_T' (dashed line) are shown for the four perpendicular viewing cases. In cases two and three, the dashed line coinsides with the solid line and thus is not visible. Note that for even the wettest cases, the thermal sampling depth is greater than the reflectivity sampling depth and for the drier cases δ_T is more than an order of magnitude bigger than δ_r.

The close agreement between δ_T and δ_T' indicates that the thermal sampling depth is primarily a function of integrals over the imaginary part of the index of refraction. The minor descrepancies which do appear result primarily from ignoring absorption of the reflecte wave within the medium. These calculations were repeated with all the imaginary parts of the indices of refraction reduced by a factor of ten. The thermal sampling depths were drastically different, as would be expected, but the reflectivity sampling depth changed by less than 25% in all cases. This indicates that the reflectivity is determined, for the most part, by gradients in the real part of the refractive index.

Thus, for understanding radiometric measurements of surfaces, two sampling depths must be considered. The reflectivity characterizes changes in the real part of the refractive index over a depth of about 1/10 to 1/7 wavelengths in the medium. The thermal radiation is characterized by a different depth δ_T which is generally larger and is substantially determined by the imaginary part of the index of refraction.

Appendix I

FORTRAN IV SUBROUTINES

The two subroutines presented here, HPLD and VPLD, calculate the electric fields and thermal weighting functions for the Horizontally and Vertically polarized layered dielectric, respectively. The number of layers to be treated is N, the angle of incidence in radians, THETA, and the wavelength is XLAM. It requires 4 complex and 1 real single precision vectors of length N. The complex numbers are signified by $. $N is the vector of complex indices of refraction of the layers. $SEP and $EM are computed by the subroutine and are the electric field solutions for the positive and negative directions, respectively. DEL is the vector of layer thicknesses; the first and last of these are not used. $P is a work vector. It contains the values of p_j^2 during computations. The values of the thermal weighting function are returned in the real part. The power reflectivity is considered to be the weighting function for the first layer.

```
      SUBROUTINE HPLU($N,$EP,$EM,DEL,$P,N,THETA,XLAM)
      IMPLICIT COMPLEX ($)
      DIMENSION$N(10),$EP(10),$P(10),$EM(10),DEL(10)
      S=SIN(THETA)
      $P(1)=(1.,0.)
      NL=N-1
      DO 10 I=2,NL
      NMAX=I
      $S=$N(1)*S/$N(I)
      $C=CSQRT((1.,0.)-$S*$S)
      ARG=DEL(I)*2*3.141592/XLAM
      $ARG=2.*ARG*$N(I)*$C*(0.,1.)
      $P(I)=CEXP($ARG)*$P(I-1)
      IF(CABS($P(I)).LT.0.0001) GO TO 20
   10 CONTINUE
   20 CONTINUE
      $EP(NMAX)=(1.,0.)
      $EM(NMAX)=(0.,0.)
      DO 40 JJ=2,NMAX
      J=NMAX-JJ+1
      $SJ=$N(1)*S/$N(J)
      $CJ=CSQRT((1.,0.)-$SJ**2)
      $SJP1=$N(1)*S/$N(J+1)
      $CJP1=CSQRT((1.,0.)-$SJP1**2)
      $A=2*$N(J)*$CJ/($N(J)*$CJ  +$N(J+1)*$CJP1)
      $B=($N(J)*$CJ-$N(J+1)*$CJP1)/(($N(J)*$CJ+$N(J+1)*$CJP1)*$P(J))
      $FP(J)=$EP(J+1)/$A+$B*$EM(J+1)/$A
      $FM(J)=$EM(J+1)+($EP(J+1)-$EP(J))*$P(J)
   40 CONTINUE
      $X=$EP(1)
      DO 45 J=1,NMAX
      $EP(J)=$EP(J)/$X
      $EM(J)=$EM(J)/$X
   45 CONTINUE
      DO 50 J=NMAX,N
   50 $P(J)=(0.,1.)/(1.E50)
      LL=NMAX-1
      DO 60 JJ=1,LL
      J=NMAX-JJ  +1
      $S=SIN(THETA)/$N(J)
      $C=CSQRT((1.,0.)-$S**2)
      R=CABS($P(J))
      S=CABS($P(J-1))
      F2=(S-R)*CABS($EP(J))**2+(1./R-1./S)*CABS($EM(J))**2
      DP=F2*REAL($N(J)*$C)/COS(THETA)
      $XP=$EP(J)*CONJG($EM(J))
      X=2.*AIMAG($N(J)*$C/COS(THETA))*(AIMAG($XP*$P(J-1)/CABS($P(J-1)))
     &-AIMAG($XP*$P(J)/CABS($P(J))))
      DP=DP-X
      $P(J)=CMPLX(DP,0.)
   60 CONTINUE
      R=CABS($EM(1))**2*REAL($N(1))
      $P(1)=CMPLX(R,0.)
      RETURN
      END
```

```
      SUBROUTINE VPLD($N,$EP,$EM,DEL,$P,N,THETA,XLAM)
      IMPLICIT COMPLEX ($)
      DIMENSION$N(10),$EP(10),$P(10),$EM(10),DEL(10)
      S=SIN(THETA)
      $P(1)=(1.,0.)
      NL=N-1
      DO 10 I=2,NL
      NMAX=I
      $S=$N(1)*S/$N(I)
      $C=CSQRT((1.,0.)-$S*$S)
      ARG=DEL(I)*2*3.141592/XLAM
      $ARG=2.*ARG*$N(I)*$C*(0.,1.)
      $P(I)=CEXP($ARG)*$P(I-1)
      IF(CABS($P(I)).LT.0.0001) GO TO 20
   10 CONTINUE
   20 CONTINUE
      $EP(NMAX)=(1.,0.)
      $EM(NMAX)=(0.,0.)
      DO 40 JJ=2,NMAX
      J=NMAX-JJ+1
      $SJ=$N(1)*S/$N(J)
      $CJ=CSQRT((1.,0.)-$SJ**2)
      $SJP1=$N(1)*S/$N(J+1)
      $CJP1=CSQRT((1.,0.)-$SJP1**2)
      $D=2.*$N(J)*$CJ
      $A=$N(J)*$CJP1+$N(J+1)*$CJ
      $B=$N(J)*$CJP1-$N(J+1)*$CJ
      $EP(J)=$A*$EP(J+1)/$D   +$B*$EM(J+1)/($D*$P(J))
      $R=$N(J+1)/$N(J)
      $EM(J)=$R*$EM(J+1)+($EP(J)-$EP(J+1)*$R)*$P(J)
   40 CONTINUE
      $X=$EP(1)
      DO 45 J=1,NMAX
      $EP(J)=$EP(J)/$X
      $EM(J)=$EM(J)/$X
   45 CONTINUE
      DO 50 J=NMAX,N
   50 $P(J)=(0.,1.)/(1.E50)
      LL=NMAX-1
      DO 60 JJ=1,LL
      J=NMAX-JJ   +1
      $S=SIN(THETA)/$N(J)
      $C=CSQRT((1.,0.)-$S**2)
      R=CABS($P(J))
      S=CABS($P(J-1))
      F2=(S-R)*CABS($EP(J))**2+(1./R-1./S)*CABS($EM(J))**2
      DP=F2*REAL($N(J)*$C)/COS(THETA)
      $XP=$EP(J)*CONJG($EM(J))
      X=2.*AIMAG($N(J)*$C/COS(THETA))*(AIMAG($XP*$P(J-1)/CABS($P(J-1)))
     &-AIMAG($XP*$P(J)/CABS($P(J))))
      DP=DP-X
      $P(J)=CMPLX(DP,0.)
   60 CONTINUE
      R=CABS($EM(1))**2*REAL($N(1))
      $P(1)=CMPLX(R,0.)
      RETURN
      END
```
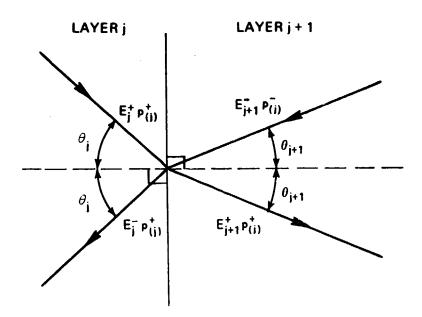
Figure 1. Schematic representation of reflected and transmitted waves at the interface between the j'th and j + 1'st layer.
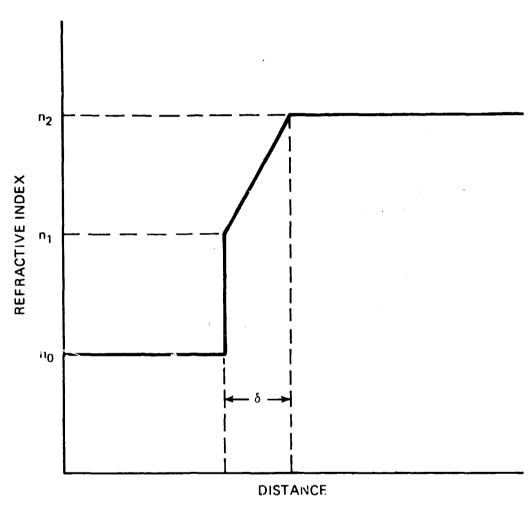
Figure 2. Schematic representation of variation of index of refraction at the interface of transmitting media.
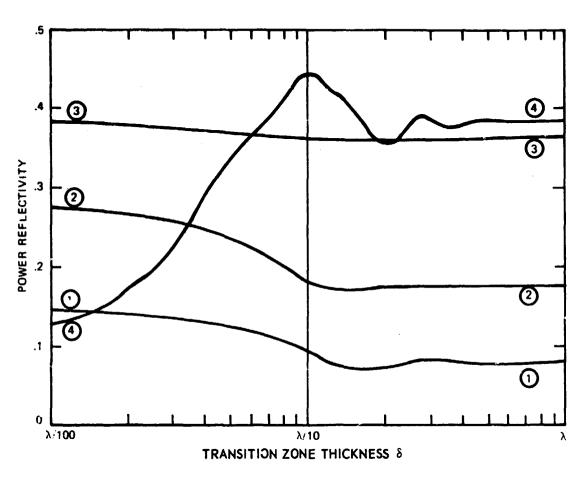
Figure 3. Power reflection at normal incidence as a function of transition zone thickness. The circled numbers by the curves give the model number (see Table 1).
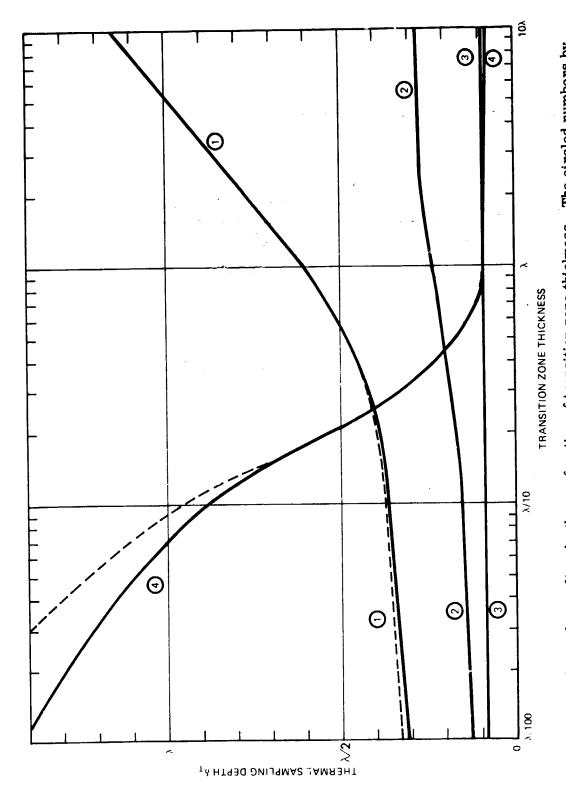
15

Figure 4. Thermal sampling depth as a function of transition zone thickness. The circled numbers by each curve give the model number (see Table 1). The solid curves give the results of the multilayer calculation; the dashed lines give the integral approximation to the thermal sampling depth.

16

Table 1
Indices of Refraction and Moisture Values

Model	n_1	% Moisture Dry Weight Basis	n_2	% Moisture Dry Weight Basis
1	1.8 + 0.05i	3	2.2 + 0.25i	12
2	2.4 + 0.28i	15	3.1 + 0.60i	20
3	3.8 + 0.90i	22	4.0 + 0.98i	25
4	4.0 + 0.98i	25	1.8 + 0.05i	3

Table 2
Convergence of Multilayer Approximation

Model	Viewing Angle	Polarization	Reflectivity Error			
			80 LAYERS	40 LAYERS	20 LAYERS	10 LAYERS
1	0°	—	.0003	.0010	.0025	.0158
1	45°	H	.0005	.0012	.0121	.0279
1	45°	V	.0002	.0005	.0012	.0099
2	0°	—	.0005	.0012	.0056	.0116
2	45°	H	.0005	.0017	.0052	.0111
2	45°	V	.0003	.0010	.0030	.0065
3	0°	—	.0001	.0003	.0007	.0017
3	45°	H	.0001	.0002	.0007	.0017
3	45°	V	.0001	.0003	.0007	.0016
4	0°	—	.0017	.0051	.0125	.0245
4	45°	H	.0017	.0052	.0126	.0297
4	45°	V	.0015	.0047	.0114	.0264

Table 3
Reflectivity Sampling Depths

Model	Viewing Angle	Polarization	δ_r/λ	$\langle n_r \rangle$	$\langle n_r \rangle \delta_r/\lambda$
1	0°	–	.066	2.0	.132
1	45°	H	.071	2.0	.142
1	45°	V	.073	2.0	.146
2	0°	–	.056	2.75	.154
2	45°	H	.056	2.75	.154
2	45°	V	.059	2.75	.162
3	0°	–	.040	3.90	.156
3	45°	H	.040	3.90	.156
3	45°	V	.040	3.90	.156
4	0°	–	.033	2.90	.096
4	45°	H	.033	2.90	.096
4	45°	V	.032	2.90	.093

REFERENCES

1. Krauss, J. D., "Radio Astronomy," (McGraw-Hill, New York) 1966

2. Panofsky, W. K. H., and M. Phillips, "Classical Electricity and Magnetism," (Addison-Wesley, Reading, Mass.) 1962

3. Schmugge, T., P. Gloersen, T. Wilheit, and F. Geiger, "Remote Sensing of Soil Moisture with Microwave Radiometers," J. Geophys. Res., 74, 317-323, Jan. 10, 1974

4. Wait, J. R., "Electromagnetic Waves in Stratified Media," (Pergammon Press, New York) 1970